THE JOURNAL OF PHYSICAL CHEMISTRY C
A JOURNAL OF THE AMERICAN CHEMICAL SOCIETY

pubs.acs.org/JPCC

Article

Tuning the Behavior of a Hydrotalcite-Supported Sulfonated Bithiophene from Aggregation-Caused Quenching to Efficient Monomer Luminescence

Estefanía Delgado-Pinar, Ana L. Costa, Isabel S. Gonçalves, Marta Pineiro, Martyn Pillinger,* and J. Sérgio Seixas de Melo*

Cite This: *J. Phys. Chem. C* 2021, 125, 8294–8303

Read Online

ACCESS | Metrics & More | Article Recommendations | Supporting Information

ABSTRACT: The synthesis, electronic spectral, and photophysical properties of a new bithiophene derivative, (2,2′-bithiophene)-3,5,5′-trisulfonic acid, α2-SO_3H, were investigated in organic or aqueous solution, in neat oil form, and in the solid state by cointercalation with different amounts of the surfactant 1-heptanesulfonate (HS) into a layered double hydroxide (LDH). In solution the fluorescence quantum yield (ϕ_F) of α2-SO_3H increases by 1 order of magnitude when compared to the unsubstituted bithiophene (α2) counterpart. However, the most dramatic change is obtained when α2-SO_3H is incorporated with HS into a Zn,Al-LDH, where values of ϕ_F up to 58% are obtained in comparison with values of 4% for neat α2-SO_3H (as an oil) and 2% for an LDH containing only α2-SO_3H. In the solid state (LDH), in addition to the monomeric form of α2-SO_3H, H- and other types of aggregates are present, which are found to be dependent on the percentage HS content. Time-resolved fluorescence studies further rationalize this behavior with single and double exponential decays mirroring the contributions of monomers and aggregates. The study validates a strategy of increasing fluorescence in the solid state by introduction of electrodonating groups and isolation of the α2-SO_3H units within the LDH structure with an appropriate surfactant (HS).

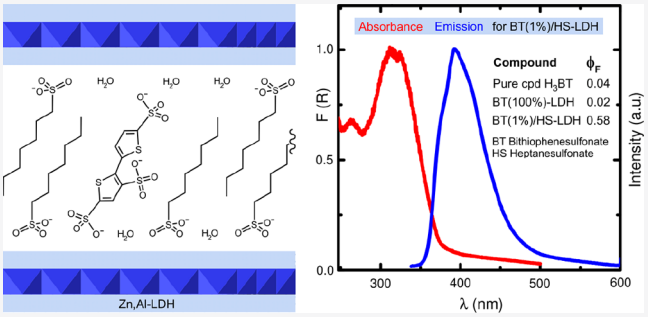

1. INTRODUCTION

Research on highly fluorescent emissive organic molecules has received increasing interest in recent years for various applications in sensors, displays, storage, and photoelectronic devices.[1−6] Thiophenes, particularly conjugated thiophene oligomers or polymers, are often used in the synthesis of optical and electronic materials owing to their good electron-transferring ability, high conductivity, and structural rigidity.[2,3,7] In fact, functional oligothiophenes have evolved as one of the most used classes of π-conjugated materials, in particular, as active components in organic electronic devices and molecular electronics.[8−10] Positional and orientational control of oligothiophenes is important for these potential applications, particularly for optimizing the efficiency of light-harvesting systems and controlling orientation-dependent charge transfer.[11−16]

However, when aggregation is not well-controlled, significant aggregation-caused quenching (ACQ) appears due to the formation of less emissive species.[17] Challenging issues are therefore to control the domain separation at a supramolecular level and the randomness in orientation of the fluorophores.[18] This approach takes its inspiration from crucial life processes where clusters or aggregates of individual elements are held together by weak intermolecular forces and are considered as single units.[19,20]

The simplest aggregate to model is the dimer. Dimers are made of two molecules and, therefore, two interacting transition dipole moments.[21] By combining dipole−dipole interactions with molecular geometry, two scenarios arise: one where the molecules are parallel with each other (H-aggregates) and the other where the monomeric units are arranged in an "in-line" fashion (J-aggregates).[21]

The self-assembly of individual organic chromophores into ordered nanostructures has been the focus of many investigations by supramolecular chemists in the last years.[22] An alternative to self-assembly of individual molecules into supramolecular aggregates is the incorporation of the organic molecules into an inorganic matrix where the spectroscopic properties of the confined emitters can be tuned to modify, for

Received: January 11, 2021
Revised: March 25, 2021
Published: April 9, 2021

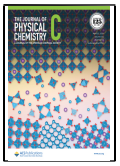

https://doi.org/10.1021/acs.jpcc.1c00240
J. Phys. Chem. C 2021, 125, 8294–8303

example, the average distance between the confined dyes, control the molecular conformation, or suppress vibrational and translational motion, among others.[18,23−26]

Layered double hydroxides (LDHs) are a class of inorganic layered materials that have received great attention due mainly to their anion exchange properties, which make them promising in such diverse fields as catalysis, corrosion inhibition, environmental remediation, UV−vis photodetection, and drug delivery.[27,28] These hydrotalcite-type materials have the general formula $[M^{2+}_{1-x}M^{3+}_{x}(OH)_2]^{x+}(A^{m-})_{x/m}\cdot nH_2O$, where M^{2+} and M^{3+} are divalent and trivalent cations, respectively, and A^{m-} is an interlayer anion with charge $-m$. The structure is derived from that of brucite $[Mg(OH)_2]$ by isomorphous replacement of some of the divalent cations by trivalent ones to give positively charged layers that require the presence of charge-balancing interlayer anions.[29] Some reports exist on the incorporation of thiophene derivatives into hydrotalcite-type materials. LDHs were used as adsorbents for thiophene removal from aqueous solution (desulfurization).[30] Tronto et al. intercalated 2-thiophenecarboxylate and 2-(thiophen-3-yl)acetate anions into Zn,Al and Zn,Cr LDHs by the direct coprecipitation method at constant pH.[31,32] The former materials were studied for their electrochemical behavior, while the latter were thermally treated to promote in situ polymerization and oligomerization of the intercalated monomers.

To the best of our knowledge, the possibility of tuning the photoluminescence behavior of functional oligothiophenes by intercalation in LDHs has not been reported. In the present work, 2,2′-bithiophene has been sulfonated in three positions with the specific aim of obtaining a derivative that could be selectively incorporated as an anionic guest in an LDH host. This structural modification proved to be a judicious choice, allowing the trisulfonated bithiophene to be intercalated in a Zn,Al LDH by a direct coprecipitation method at constant pH. To modify the microenvironment and, hence, the photophysical properties of the incorporated anions, composite materials were prepared in which the sulfonated bithiophene and a surfactant were cointercalated in different proportions. The synthetic strategy leads to an enhancement of the photoluminescence of the sulfonated bithiophene in the solid state.

2. EXPERIMENTAL SECTION

2.1. Materials and Methods. The chemicals chlorosulfonic acid, sodium bicarbonate, *tert*-butylamine, $Zn(NO_3)_2\cdot 6H_2O$ (98%, Fluka), $Al(NO_3)_3\cdot 9H_2O$ (98.5%, Riedel de-Haën), 1 M NaOH (Fluka), and 1-heptanesulfonic acid sodium salt (98%, Sigma-Aldrich) were obtained from commercial sources and used as received. 2,2′-Bithiophene was purified by sublimation with a coldfinger. Water was twice distilled and passed through a Millipore apparatus. All the solvents (spectroscopic or equivalent grade) were used without further purification. The pH values were measured with a Jenway 3510 pH meter, and adjustments of the hydrogen ion concentration of the solutions were made with dilute $HClO_4$ and NaOH solutions. All LDH preparations were performed under a nitrogen atmosphere using deionized and decarbonated (DD) water. The preparation and characterization of Zn,Al LDHs intercalated by nitrate $(Zn_4Al_2(OH)_{12}(NO_3)_2\cdot 2.5H_2O$, denoted NO_3-LDH) and 1-heptanesulfonate $(Zn_4Al_2(OH)_{12}(C_7H_{15}O_3S)_{1.7}(CO_3)_{0.15}\cdot 5.5H_2O$, denoted HS-LDH) were described previously.[33]

^1H and ^{13}C NMR spectra were recorded on a Bruker-AMX spectrometer with operating frequencies of 400 and 101 MHz, respectively. High-resolution mass spectrometry (HRMS) was performed on a Bruker microTOF-Focus mass spectrometer equipped with an electrospray ionization time-of-flight (ESI-TOF) source. Solid-state ^{13}C cross-polarization (CP) magic-angle spinning (MAS) NMR spectra were recorded using a wide-bore Bruker Avance III 400 spectrometer (9.4 T) at 100.62 MHz with 3.7 μs ^1H 90° pulses, 3500 ms contact time, spinning rates of 12 kHz, and 5 s recycle delays.

Microanalyses for C, H, and N were carried out with a Truspec Micro CHNS 630−200−200 elemental analyzer. Powder X-ray diffraction (PXRD) data were collected at ambient temperature on a Philips Analytical Empyrean diffractometer equipped with a PIXcel 1D detector, with automatic data acquisition (X'Pert Data Collector software version 4.2) using monochromatized Cu K_α radiation (λ = 1.54178 Å). Intensity data were collected by the step-counting method (step 0.02°), in continuous mode, in the 2θ range 3−70°. Scanning electron microscopy (SEM) images were obtained on a Hitachi SU-70 microscope at 15 kV. Samples were prepared by deposition on aluminum sample holders, followed by carbon coating using an Emitech K 950 carbon evaporator. TGA was performed using a Shimadzu TGA-50 system at a heating rate of 5 °C min^{-1} under air. FT-IR spectra were collected using KBr pellets and a Mattson-7000 infrared spectrophotometer.

Absorption spectra were obtained with a Cary 5000 spectrophotometer. Excitation and emission spectra were recorded in solution and the solid state with a Horiba-Fluoromax-4 spectrofluorimeter. All the fluorescence spectra were corrected for the wavelength response of the system. The fluorescence quantum yields were measured using the absolute method with a Hamamatsu Quantaurus QY absolute photoluminescence quantum yield spectrometer model C11347 (integration sphere). The absorption of the solutions was kept under 0.1 at the excitation wavelength to avoid the inner filter effect.[34] Fluorescence decay times were obtained by the Time-Correlated Single Photon Counting (TCSPC) technique with nanosecond and picosecond time resolution using equipment described elsewhere.[35,36] The fluorescence decays obtained were deconvoluted by employing the method of modulating functions implemented by George Striker.[37]

The fluorescence intensity response with time, $I(t)$, is given by eq 1 with decay times τ_1 and τ_2 and pre-exponential factors (a_1 and a_2) mirroring the excited state concentrations at time zero:

$$I(t) = a_1 e^{-t/\tau_1} + a_2 e^{-t/\tau_2} \quad (1)$$

The fractional contribution (C_i) of each lifetime is an additional parameter obtained from the decays that allows a better interpretation of these results. The C_i, in Table 3 below, for each species (1 and 2) is given by the following equation:[38]

$$C_i(\%) = \frac{a_i\tau_i}{\sum_{i=1}^{n} a_i\tau_i} \times 100 \quad (2)$$

where n stands for the number of exponential terms, a_i is the contribution of each exponential term at t = 0, and τ_i is the associated decay times.

Structural models and representations were generated using CrystalMaker software.[39]

https://doi.org/10.1021/acs.jpcc.1c00240
J. Phys. Chem. C 2021, 125, 8294−8303

Scheme 1. Synthetic Route for the Trisulfonic Acid Derivative[a]

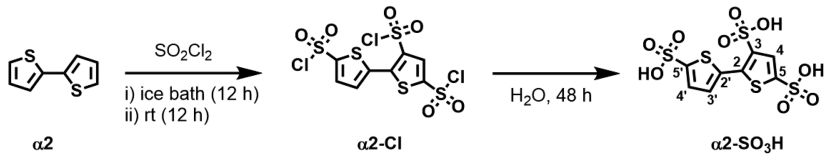

[a]The atom numbering for the NMR assignments is included.

2.2. Synthesis. *(2,2′-Bithiophene)-3,5,5′-trisulfonyltrichloride, α2-Cl.* 2,2′-Bithiophene (*α*2; 0.6 g, 3.61 mmol) was placed in a round-bottom flask under nitrogen in an ice bath. Keeping an inert atmosphere, chlorosulfonic acid (13 mL, 180 mmol) was added. The mixture was stirred at 0 °C for 12 h and then overnight at room temperature. The solution was neutralized with saturated $NaHCO_3$ (aq), and the solid was then filtered and washed with water (2.01 g, 82% yield (90% purity by NMR)).

^{1}H NMR (DMSO, 400 MHz): δ (ppm) = 7.04 (d, J = 3.7 Hz, 1H), 7.22 (s, 1H), 7.49 (d, J = 3.7 Hz, 1H).

^{13}C NMR (DMSO, 101 MHz): δ (ppm) = 126.4, 128.1, 129.3, 132.3, 134.3, 142.9, 146.4, 151.0.

(2,2′-Bithiophene)-3,5,5′-trisulfonic acid, α2-SO$_3$H. The chlorosulfonic acid intermediate *α*2-Cl was suspended in 500 mL of water for 48 h under vigorous stirring until an orange solution was obtained. After water evaporation under vacuum, the orange-brown oil obtained was dried at 100 °C for 12 h and purified by column chromatography, TLC (SiO_2, CH_2Cl_2/methanol/isopropylamine, 60:40:drops) to provide the desired compound *α*2-SO_3H.

^{1}H NMR (MeOD, 400 MHz): δ (ppm) = 7.36 (d, J = 3.9 Hz, 1H), 7.58 (d, J = 3.9 Hz, 1H), 7.66 (m, 1H), 7.85 (m, 0.23H).

^{13}C NMR (MeOD, 101 MHz): δ (ppm) = 129.1, 130.0, 131.1, 136.4, 136.9, 141.9, 145.8, 149.7.

ESI-MS (m/z): Calcd for $C_8H_6O_9S_5$: 406.46. Found: $[L - H]^-$, 404.8576; $[L + Na^+ - 2H]^-$, 426.8399; $[L + Na^+ + K^+ - 2H]^-$, 463.9311.

HSQC NMR spectra of *α*2-SO_3H are given in Figure S2.

2.3. LDH Composites Synthesis. *α2-SO$_3$-LDH.* An aqueous solution (20 mL) of the sodium salt of *α*2-SO_3H was prepared by mixing *α*2-SO_3H (0.32 g, 0.79 mmol), 0.35 M NaOH (3 equiv) and water. A solution of $Zn(NO_3)_2{\cdot}6H_2O$ (0.47 g, 1.57 mmol) and $Al(NO_3)_3{\cdot}9H_2O$ (0.30 g, 0.79 mmol) in deionized water (DD) water (20 mL) was added dropwise to the solution of *α*2-SO_3Na under vigorous mixing. During the addition of the Zn^{2+}/Al^{3+} solution, the pH of the reaction mixture was maintained at 8.4 by dropwise addition of 0.35 M NaOH. After the addition was complete, the resultant dark yellow suspension was aged at 65 °C for 18 h. The solid product was filtered, washed with DD water (5 × 100 mL), and finally dried at room temperature in a vacuum desiccator. Analysis calculated for $Zn_4Al_2(OH)_{12}(C_8H_3O_9S_5)_{0.56}(NO_3)_{0.02}(CO_3)_{0.15}{\cdot}5H_2O$ (845.85): C, 6.57; H, 2.82; N, 0.03; S, 10.61. Found: C, 6.59; H, 2.67; N, 0.03; S, 10.28. TGA showed a mass loss of 9.9% at 150 °C (calcd for $5H_2O$: 10.6%). FT-IR (KBr, cm^{-1}): ν = 3473 (br), 2931 (w), 2857 (w), 1630 (s), 1500 (w), 1415 (m), 1385 (w), 1202/1222 (vs), 1099 (m), 1072 (s), 1049 (s), 1012 (w), 889 (w), 719 (w), 688 (m), 644 (m), 611 (s), 553 (w), 425 (s), 316 (w). ^{13}C{^{1}H} CP MAS NMR: δ = 148.2, 143.2, 137.9, 133.7, 129.2 ppm.

α2-SO$_3$(n%)/HS-LDH Composites. Aqueous solutions (80 mL) of the sodium salt of *α*2-SO_3H were prepared by mixing *α*2-SO_3H, 0.35 M NaOH (3 equiv), and water. Two solutions (A and B) were prepared containing different amounts of 1-heptanesulfonic acid sodium salt (*a* mmol) and *α*2-SO_3Na (*b* mmol; *a* + *b* = 10 mmol; *b* = 0.23 (solution A) or 0.046 (solution B) mmol). A solution of $Zn(NO_3)_2{\cdot}6H_2O$ (2.97 g, 10 mmol) and $Al(NO_3)_3{\cdot}9H_2O$ (1.88 g, 5 mmol) in DD water (60 mL) was added dropwise to solution A or B with vigorous mixing. During the addition of the Zn^{2+}/Al^{3+} solution, the pH of the reaction mixture was maintained at 8.20−8.45 by the dropwise addition of 0.35 M NaOH. After the addition was complete, the resultant gel-like slurry was aged at 65 °C for 18 h. The solid product was filtered, washed with DD water (5 × 100 mL), and finally dried at room temperature in a vacuum desiccator. The samples are denoted as *α*2-SO_3(*n*%)/HS-LDH, where the final mol % content of *α*2-SO_3 (*n*) is calculated by considering that uptake of the trianion of *α*2-SO_3H in the synthesized LDH will be selective and quantitative and that the remaining layer positive charge will be compensated by cointercalated HS anions.

3. RESULTS AND DISCUSSION

3.1. Synthesis and Characterization. *α2-SO$_3$H.* Scheme 1 depicts the procedure used for the synthesis of the novel bithiophene derivative (2,2′-bithiophene)-3,5,5′-trisulfonic acid (*α*2-SO_3H). Briefly, chlorosulfonation of bithiophene (*α*2) through electrophilic aromatic substitution with neat chlorosulfonic acid at 0 °C during 24 h gave the trisulfonyl chloride derivative *α*2-Cl as a dark brown solid in almost quantitative yield.[40] The resulting solid was then suspended in water for 48 h to hydrolyze the chlorosulfonic groups. Finally, the product *α*2-SO_3H was obtained as an oil by solid chromatography purification. Attempts to get crystals of *α*2-SO_3H or the corresponding sodium salts have been unsuccessful.

LDHs. Zn,Al layered double hydroxides (LDHs) containing solely the trisulfonate derivative *α*2-SO_3 (*α*2-SO_3-LDH) or 1-heptanesulfonate (HS) anions (HS-LDH), or a mixture with two different *α*2-SO_3/HS molar ratios (ca. 1.0 and 5.0 mol % *α*2-SO_3, samples *α*2-SO_3(1%)/HS-LDH and *α*2-SO_3(5%)/HS-LDH) were prepared by the direct coprecipitation method at constant pH.

The PXRD pattern of *α*2-SO_3-LDH displays four fairly broad, equally spaced, symmetric peaks between 3.5 and 30° 2θ, which are assigned as the 00l reflections of a hydrotalcite-type layered phase (Figure 1). The basal (interlayer) spacing (d_b) can be calculated from averaging the positions of the four harmonics: $d_b = 1/4(d_{003} + 2d_{006} + 3d_{009} + 4d_{0012}) = 13.75$ Å. Relatively weak and asymmetric peaks above 30° 2θ are assigned as overlapping nonbasal reflections. The gallery height in *α*2-SO_3-LDH is estimated as 9.0 Å by the subtraction of 4.75 Å for the layer thickness from the basal spacing. A model

https://doi.org/10.1021/acs.jpcc.1c00240
J. Phys. Chem. C 2021, 125, 8294−8303

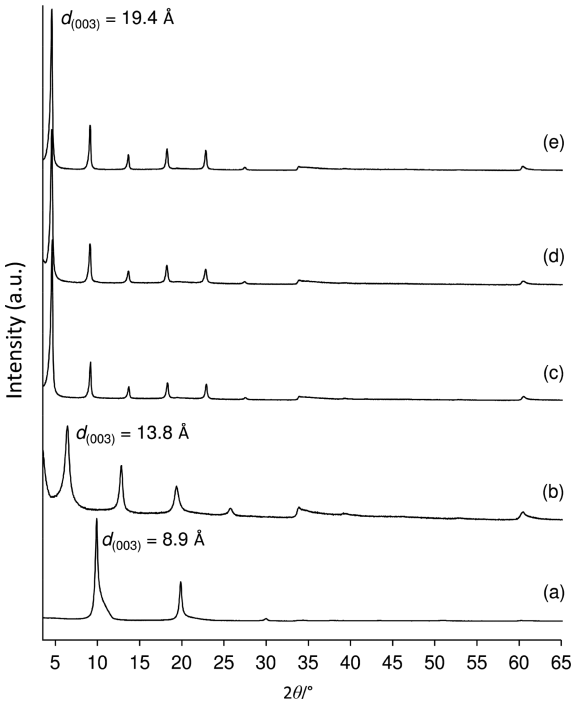

Figure 1. PXRD patterns of (a) NO_3-LDH, (b) α2-SO_3-LDH, (c) HS-LDH, (d) α2-SO_3(5%)/HS-LDH, and (e) α2-SO_3(1%)/HS-LDH.

for the molecular structure of the anion (2,2′-bithiophene)-3,5,5′-trisulfonate, with realistic bond lengths and overall geometry, was generated by extracting relevant structural features from two crystal structures deposited in the Cambridge Crystal Database (CSD):[41] CSD-ROFLIK (containing the anion 5-bromothiophene-2-sulfonate) and CSD-QEDMAQ (containing the anion 2,2′-bithiophene-5,5′-dicarboxylate).[42] A credible model for the interlayer orientation of the bithiophene guest in α2-SO_3-LDH can be advanced by considering that the following criteria must be met: (i) hydrogen-bonding interactions between the sulfonate oxygen atoms and the layer hydroxyl groups should be maximized, while positioning the hydrophobic bithiophene moiety in the center of the interlayer region; (ii) the orientation must be consistent with a gallery height of 9.0 Å (taking into account van der Waals (vdW) radii for the sulfonate oxygen atoms); (iii) the anionic guest must be spatially capable of compensating the host layer positive charge. Figure 2 shows an interlayer arrangement that meets these requirements. In this orientation, the cross-sectional area occupied by the guest molecules in a plane parallel with the layers is estimated as 71 $Å^2$, which corresponds to an area per unit charge of 23.7 $Å^2$. The area per unit charge for an LDH is given by $(1/x)a_0^2 \sin 60°$, where x is the mole fraction $[Al^{3+}]/[Zn^{2+} + Al^{3+}]$, and a_0 is the hexagonal unit cell parameter. For an LDH with Zn/Al = 2, x = 0.33 and $a_0 \sim 3.1$ Å, which lead to a calculated area per unit positive charge of 25.0 $Å^2$. For this simplified model, the average perpendicular distance between thiophene planes of adjacent molecules is estimated as 5.6 Å. Hence, a monolayer of closely packed (2,2′-bithiophene)-3,5,5′-trisulfonate anions, as depicted in Figure 2, should be fully capable of compensating the host layer charge. Finally, the perpendicular interplanar distance between adjacent bithiophene guest molecules in α2-SO_3-LDH (estimated as 5.6 Å) is too large to produce effective $\pi-\pi$ intermolecular electronic coupling.

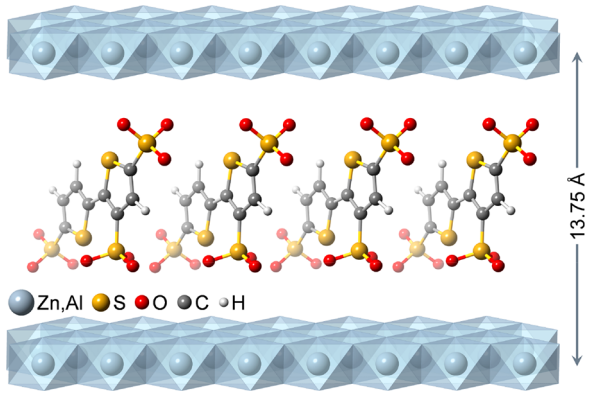

Figure 2. Structural model for the monolayer arrangement of bithiophene guests in the material α2-SO_3-LDH.

The PXRD patterns of the materials HS-LDH and α2-SO_3(n %)/HS-LDH are very similar, showing six fairly sharp, equally spaced, symmetric 00l reflections between 3.5 and 30° 2θ, from which a basal spacing of 19.4 Å is calculated for all three materials (Figure 1). As reported previously for HS-LDH, this basal spacing is most likely to arise from an ordered interlayer packing arrangement in which the surfactant molecules adopt an almost perpendicular (or slightly tilted) bilayer arrangement with extensive interdigitation (i.e., an antiparallel interpenetrating style).[33] None of the patterns contain basal reflections characteristic of nitrate-LDH or carbonate-LDH phases. Also, the sample with the higher loading of α2-SO_3H does not display any weak reflections corresponding to an LDH phase intercalated solely by the bithiophene guest, that is, with $d_{003} \sim 13.8$ Å.

The phase purity of the materials α2-SO_3-LDH and α2-SO_3(n%)/HS-LDH was further checked by SEM (Figure S1). The morphology of the intercalated LDHs consisted of aggregates of irregular sheet-like nanoparticles. No evidence was found for secondary phases such as ZnO or Al_2O_3.

Figure 3 shows the FT-IR spectra of the intercalated materials. In the region of the S−O stretching vibrations (900−1450 cm^{-1}), the spectra of α2-SO_3-LDH and α2-SO_3(n %)/HS-LDH (n = 0, 1.0, and 5.0%) are typical of dissociated sulfonate groups with a broad peak at 1179 cm^{-1} or doublet at about 1202/1222 cm^{-1} (asymmetric SO_3^- stretching vibration for HS and α2-SO_3, respectively) and a sharper absorption at 1049 cm^{-1} (symmetric SO_3^- stretching vibration). The corresponding spectra for the neat compounds α2-SO_3H and NaHS are similar, showing bands centered at 1056 and 1190 cm^{-1} for NaHS and 1046 and 1202 cm^{-1} for α2-SO_3H. The spectrum for α2-SO_3H does not contain bands typical of undissociated sulfonic acid groups (asymmetric SO_2 stretching mode at ca. 1400 cm^{-1} and S−O stretching mode at ca. 900 cm^{-1}). This can be attributed to the presence of water and ionization of the SO_3H groups to give sulfonate−hydronium ionic pairs, which will present S−O stretching vibrations that resemble those for sulfonate salts. Figure 3 shows that the FT-IR spectra for the two samples containing about 1.0 and 5.0 mol % α2-SO_3H are practically identical and that bands assignable to the bithiophene guest species are not visible. These bands are obscured by the absorptions due to the cointercalated HS anions, even for the sample with the higher α2-SO_3H loading.

In the region 300−650 cm^{-1}, the FT-IR spectra of α2-SO_3-LDH and α2-SO_3(n%)/HS-LDH present three main

https://doi.org/10.1021/acs.jpcc.1c00240
J. Phys. Chem. C 2021, 125, 8294−8303

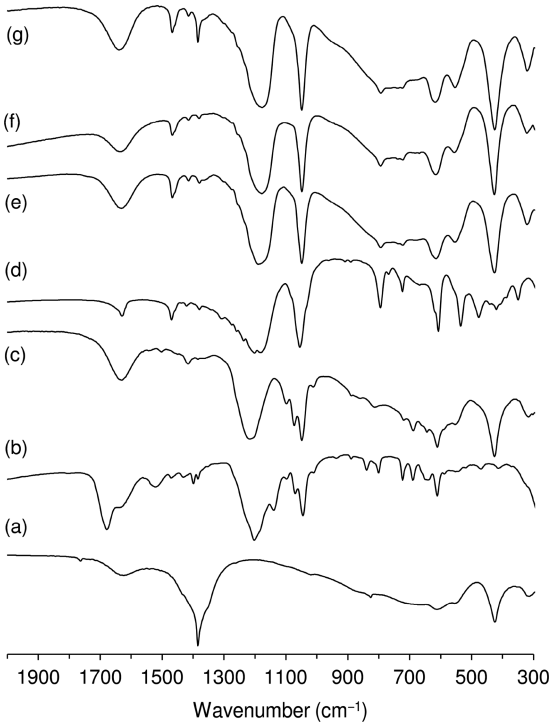

Figure 3. FT-IR spectra in the region 300−2000 cm^{-1} of (a) NO_3-LDH, (b) α2-SO_3H, (c) α2-SO_3-LDH, (d) NaHS, (e) HS-LDH, (f) α2-SO_3(5%)/HS-LDH, and (g) α2-SO_3(1%)/HS-LDH.

bands at about 425, 555, and 615 cm^{-1}, which are attributed to the characteristic Zn/Al−OH lattice translation modes of Zn,Al LDHs. Similar bands are observed for the nitrate-form material NO_3-LDH (Figure 3a). The spectra indicate that the samples only contain minor or insignificant amounts of carbonate or nitrate ions (characteristic bands: $\nu_3(CO_3^{2-}) \sim 1365$ cm^{-1}, $\nu_3(NO_3^-) \sim 1385$ cm^{-1}).

The solid-state $^{13}C\{^1H\}$ CP MAS NMR spectrum of α2-SO_3-LDH displays five resolved broad lines and several shoulders in the aromatic region between 110 and 160 ppm (Figure 4a). These signals can be assigned in accordance with the liquid ^{13}C NMR spectrum of α2-SO_3H which displays five main groups of resonances attributed to C^2, $C^{2\prime}$, $C^{5\prime}$, $C^{3,5}$, and $C^{3\prime,4,4\prime}$ (Figure 4). The $^{13}C\{^1H\}$ CP MAS NMR spectra of α2-SO_3(n%)/HS-LDH (n = 0, 1.0, and 5.0%) are very similar in the aliphatic region (10−40 ppm), exhibiting six single peaks for the carbon atoms of the n-heptyl group (C^3 and C^4 are not resolved as separate resonances). In contrast, while the spectrum of NaHS also displays a single line for the methyl carbon atom (C^7), multiple sharp resonances are observed for each type of methylene carbon atom (Figure 4b), possibly due to conformational heterogeneity in the solid state. The spectra of the HS-containing LDHs are therefore consistent with an ordered, essentially all-anti, conformation of the methylene chains. In accordance with the FT-IR data, signals due to the cointercalated biothiophene guest could not be discerned in the ^{13}C NMR spectra of α2-SO_3(n%)/HS-LDH (n = 1.0 and 5.0%).

The thermal decomposition behaviors of α2-SO_3-LDH and α2-SO_3(n%)/HS-LDH (n = 1.0 and 5.0%) were examined by TGA (Figure 5). For α2-SO_3-LDH, the weight loss of 9.9% from ambient temperature up to 150 °C is due to the removal of physisorbed and interlayer water molecules. From this water content and CHN microanalyses, the formula

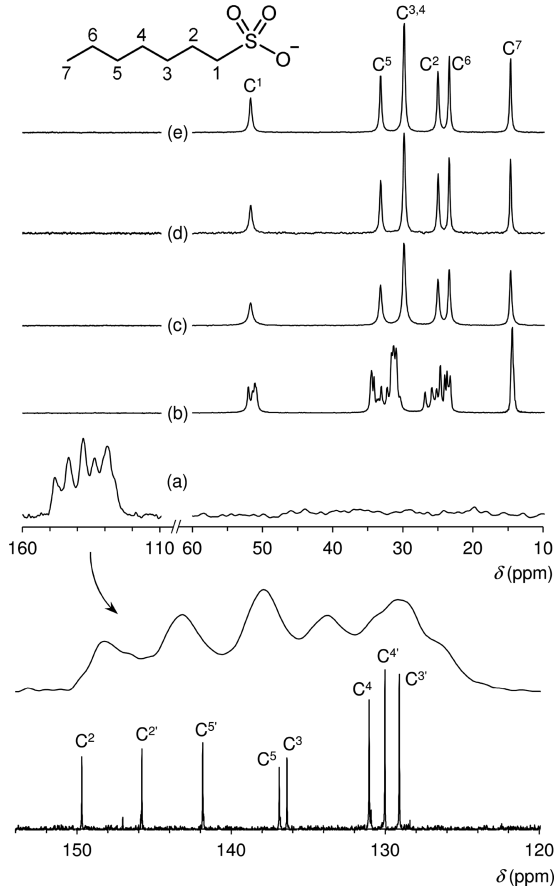

Figure 4. $^{13}C\{^1H\}$ CP MAS NMR spectra of (a) α2-SO_3-LDH, (b) NaHS, (c) HS-LDH, (d) α2-SO_3(5%)/HS-LDH, and (e) α2-SO_3(1%)/HS-LDH. A magnified view of the aromatic region for spectrum (a) is shown and compared with the liquid ^{13}C NMR spectrum of α2-SO_3H in MeOD. Scheme 1 shows the carbon atom numbering for α2-SO_3H.

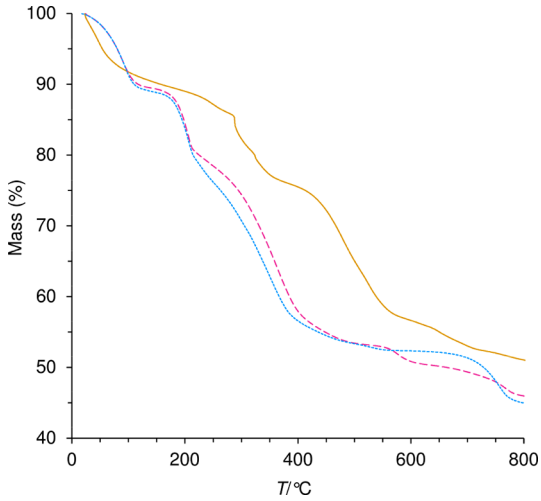

Figure 5. TGA curves for α2-SO_3-LDH (yellow solid line), α2-SO_3(5%)/HS-LDH (red dash line), and α2-SO_3(1%)/HS-LDH (blue dash line).

$Zn_4Al_2(OH)_{12}(C_8H_3O_9S_5)_{0.56}(NO_3)_{0.02}(CO_3)_{0.15}\cdot 5H_2O$ is proposed for the as-prepared organic−inorganic hybrid. Upon further heating, dehydroxylation of the host hydroxide layers gives rise to a weight loss step of 8.6% between 280 and 350

https://doi.org/10.1021/acs.jpcc.1c00240
J. Phys. Chem. C 2021, 125, 8294−8303

°C, which is followed by a 16.6% weight loss between 400 and 550 °C corresponding to thermal decomposition of the intercalated bithiophene guest. The TGA curves for α2-SO_3(n%)/HS-LDH (n = 1.0 and 5.0%) are similar to that described previously for HS-LDH.[33] Three main weight loss steps are observed from ambient temperature up to 500 °C: loss of water up to 130 °C (10.4−10.8%), dehydroxylation between 165 and 225 °C (8.9−9.7%), and surfactant decomposition between 225 and 450 °C (24.2−25.4%).

3.2. Absorption and Fluorescence Studies. Absorption and fluorescence emission spectra for α2-SO_3H were obtained in water and methanol and are depicted in Figure 6 (see Figure S4 for other spectra, including the excitation spectra). In general, the spectra of α2-SO_3H display the characteristic features of the parent oligothiophene (with a broad absorption band, lacking vibronic structure, and a more structured fluorescence emission).

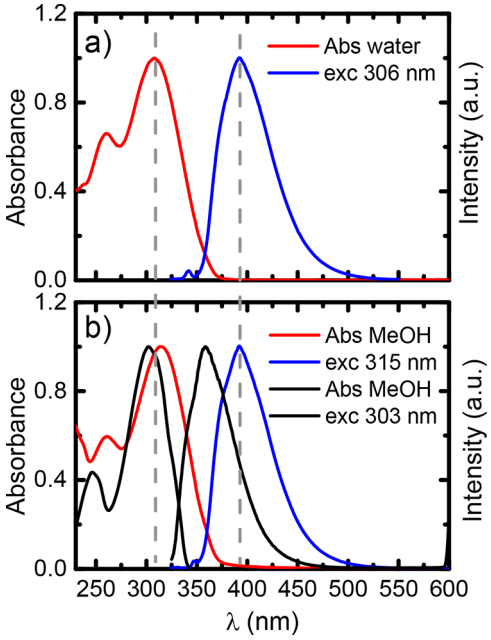

Figure 6. Normalized absorption and fluorescence emission spectra of (a) α2-SO_3H in water at pH ∼ 5.5 (λ_{exc} = 306 nm) and (b) α2-SO_3H together with α2 (black lines) in methanol; excitation wavelengths, λ_{exc}, are 306 nm in water and 315 nm in MeOH for α2-SO_3H and 303 nm for α2. obtained at T = 293 K. [α2-SO_3H] = 1 × 10^{-5} M. The vertical dashed lines are visual guides.

Table 1 gives the spectral data and the fluorescence quantum yields for α2-SO_3H in water and methanol, with literature data for α2 included for comparison. A blue-shift with the increase in the polarity of the media is observed in the absorption spectra, whereas no observable change in the fluorescence is found. These results point, as with α2, to a quinoidal-like structure in the excited state of α2-SO_3H and likely the presence of a transition with a partial intramolecular charge transfer character; the similar Stokes' shift value of α2-SO_3H and α2 (Table 1) likely indicates the same nature in the transition and excited state.[43] Indeed, α2-SO_3H exhibits large spectral solvent-dependent red-shifts of the absorption and emission wavelength maxima when compared to α2 (see Table 1 and Figure 6). The spectral shape of the absorption and emission spectra of α2-SO_3H are relatively similar to those of α2, with a broad and devoid of vibronic resolution absorption and an emission with a vibronic shoulder at shorter wavelengths. Furthermore, the addition of sulfonic acid groups in the structure of bithiophene results in a 10-fold increase in the absolute quantum yield in the case of methanol (reported to be 0.01 for α2 in ethanol) and a 20-fold increase when dissolved in water.[43]

pH-Dependence Studies. The derivatization of the bithiophene unit with sulfonic acid groups increases the solubility in water, which makes it possible to study the spectroscopic and photophysical properties of α2-SO_3H across a wide pH range. Figure 7 shows that no changes in the absorbance and emission spectral profiles are observed on going from low to intermediate and to high pH values, indicating that no protonation of the sulfonate group has occurred under these experimental conditions (please see Figure S5 in the Supporting Information for additional pH values).

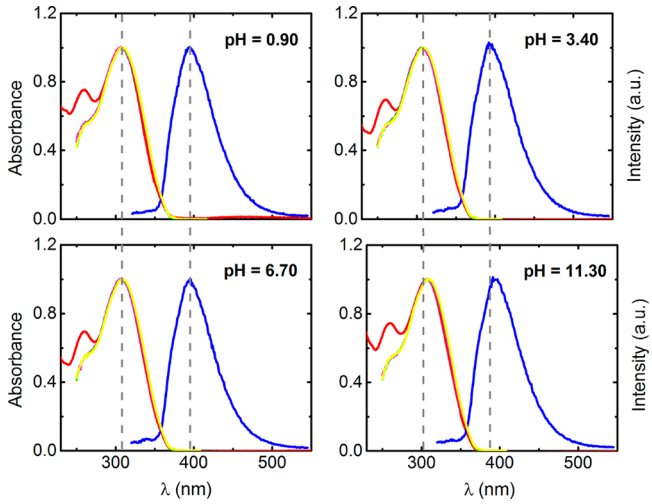

Figure 7. Normalized absorption (red), fluorescence excitation (λ_{em} = 370 nm yellow; λ_{em} = 394 nm green; λ_{em} = 430 nm pink; these show an almost full overlap), and fluorescence emission spectra (λ_{exc} = 275 nm blue) of α2-SO_3H in water at different pH values at T = 293 K. [α2-SO_3H] = 1 × 10^{-5} M. The vertical dashed lines are visual guides.

3.3. Time-Resolved Fluorescence Measurements. Time resolved fluorescence studies provided additional

Table 1. Spectral Data (Including Absorption, λ_{abs}, Excitation, λ_{exc} (Maximum Obtained from the Excitation Spectra), and Emission, λ_{em}, Wavelength Maxima; Stokes Shifts and Quantum Yield, ϕ_F, for α2 and α2-SO_3H at T = 293 K

compound	solvent	η^b (cP)	ε'^c	λ_{Abs} (nm)	λ_{em} (nm)	λ_{exc} (nm)	Stokes shift (cm^{-1})	ϕ_F
α2[a]	MeOH	0.593	32.66	302	358	302	5180	0.014
α2-SO_3H	MeOH	0.593	32.66	315	393	315	6301	0.12
	H_2O	1.009	80.16	308	393	307	7128	0.20

[a]Data for ϕ_F is in ethanol from ref 43. [b]η = viscosity. [c]ε' = dielectric constant of the solvent.

https://doi.org/10.1021/acs.jpcc.1c00240
J. Phys. Chem. C 2021, 125, 8294−8303

information on the excited state behavior of α2-SO_3H. The fluorescence decays of α2-SO_3H in water at different pH values were obtained with excitation at 275 nm and emission at 393 nm at T = 293 K. The study of the variation of the decay time values for α2-SO_3H at different pH values was carried out. No changes in the maximum wavelength allow us to verify that the sulfonate groups remained deprotonated over the whole pH range studied (see Experimental Section for further information, eq 1). The fluorescence decay times and pre-exponential factors obtained as a function of pH are depicted in Figure S6 and values are collected in Table S1. The two components, showing dependence with pH, are associated with short (varying between 190 and 250 ps) and long (varying between 400 and 600 ps) decay times. The larger difference is observed at pH < 0. However, the most interesting feature is the dependence of the pre-exponential factors on pH, where it can be seen that the a_1 pre-exponential factor decreases, whereas a_2 increases with pH, plateauing from pH = 4 thereon.

This contrasts with the single exponential behavior of the model compound α2 and likely indicates the presence of two species or two (structurally similar) compounds. Indeed, with α2, an ensemble of conformers are present in the ground state with the dominant with a dihedral angle of ~20°, whereas in the excited state a quinoidal structure is present, with a monoexponential decay. The biexponential nature of the decay of α2-SO_3H suggests the presence of two stable conformers in the ground and excited states. The emission spectra in solution is found independent of the excitation wavelength (Figure 7). This indicates that the emission is observed from a common chromophore unit (basically identified with α2), but that a mixture of two different trisulfonated derivatives of α2-SO_3H may be present and would explain the absence of total overlap of the absorption and excitation spectra in the 250−270 nm region.

3.4. Spectral and Photophysical Study of LDH-Supported α2-SO_3. As shown above, derivatization of bithiophene with sulfonic acid groups increases the solubility of the compound and strongly promotes the deactivation of the S_1 excited state through the fluorescence channel.

Immobilization of α2-SO_3 inside the LDH interlamellar region with and without surfactant spacers can further promote a change in the balance between monomer and dimer formation. The identification of the type of aggregates is relevant to the interpretation of the organization of the intercalated α2-SO_3 guests. If parallel with each other (H-aggregates or H-type dimers), the absorption spectrum is blue-shifted compared to the individual monomer. An important feature of H-type dimers is that their fluorescence is quenched. On the other hand, J-aggregates or J-dimers are characterized by absorption and emission spectra that are red-shifted relative to those for the monomeric unit,[18,44] with sharp and featureless spectra with very small Stokes shifts. However, as will be shown below, the increase of fluorescence in our systems is not due to the formation of J-aggregates, but rather to the suppression of H-aggregate formation, and thus of ACQ, by cointercalation of α2-SO_3 with a large excess of HS surfactant, leading to the emission of isolated α2-SO_3 guest anions.

UV−vis and emission spectra were collected for the solid samples α2-SO_3-LDH and α2-SO_3(n%)/HS-LDH (n = 1.0 and 5.0%) and are presented in Figure 8; for the excitation spectra, please see Figures S7 and S8. From the absorption spectra, three bands are observed: at shorter wavelengths, a band at around 260 nm together with a second (and more intense)

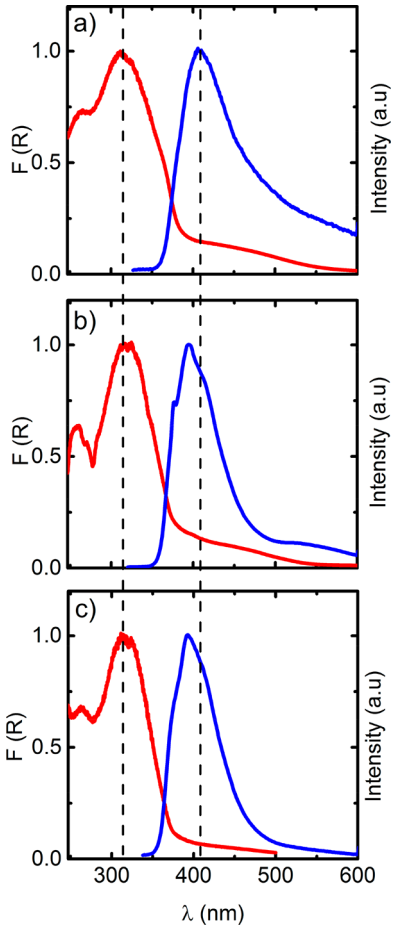

Figure 8. Normalized absorbance (red lines) and emission (blue lines) of (a) α2-SO_3-LDH, (b) α2-SO_3(5%)/HS-LDH, and (c) α2-SO_3(1%)/HS-LDH. λ_{exc} = 306 nm. The absorption spectrum of the sample containing 0% of surfactant was obtained by "diluting" the solid with $BaSO_4$.

band centered at 318 nm, and at longer wavelengths, a band (appearing as a shoulder) with a maxima at ~452 nm. The existence of these three bands in the solid state (note that for the LDH in the absence of HS surfactant the three bands are present) likely indicates the simultaneous presence of the monomer, with bands at ~260 and 318 nm, which are also found present in solution, see Figure 6, and of aggregates (band at 452 nm). Table 2 shows that the ϕ_F values for neat

Table 2. Fluorescence Quantum Yields, ϕ_F, Obtained for the Different Solid-State Samples

compound	ϕ_F
α2-SO_3(1%)/HS-LDH	0.58
α2-SO_3(5%)/HS-LDH	0.33
α2-SO_3-LDH	0.02
α2-SO_3H[a]	0.04

[a]Pure compound, a viscous oil at room temperature.

α2-SO_3H (a viscous oil at room temperature) and α2-SO_3-LDH are approximately identical. The gradual addition of the surfactant (HS) to the LDH system leads to an increase in emission from the solid. Increasing the amount (and proportion relative to α2-SO_3) of HS leads to an increase in the formation of the monomer and a reduction of H-aggregates

https://doi.org/10.1021/acs.jpcc.1c00240
J. Phys. Chem. C 2021, 125, 8294−8303

Table 3. Time Resolved Fluorescence Data (Lifetimes, τ_i, Pre-Exponential Factors, a_i, and χ-Squared Values, χ^2) for the Different Solid-State Samples[a]

compound	τ_1 (ns)	τ_2 (ns)	a_1	a_2	χ^2	$\%C_1$	$\%C_2$
α2-SO_3H[b]	0.43		1		0.82	100	
α2-SO_3-LDH	0.25	1.32	0.927	0.073	0.70	70.63	29.34
α2-SO_3(5%)/HS-LDH	0.45	1.22	0.776	0.217	1.06	56.88	43.12
α2-SO_3(1%)/HS-LDH[c]	0.42	1.21	0.809	0.004	0.93	98.60	1.40

[a]The decays were obtained with λ_{exc} = 282 nm and λ_{em} = 393 nm at T = 293 K. [b]Obtained for the pure compound, a viscous oil at room temperature. [c]An additional long-lived component associated with a baseline is present in this decay.

associated with quenching of the fluorescence (see Table 2). The emission spectra of α2-SO_3-LDH and that of α2-SO_3(5%)/HS-LDH display an additional broad band with maxima at around 550 nm, which may be attributed to the emission of the H-aggregates. For the material with the highest relative proportion of HS surfactant, α2-SO_3(1%)/HS-LDH, this band disappears, as does the longest wavelength absorption band, indicating that at a level of 1% of α2-SO_3, the surfactant "isolates" the molecule inside the LDH galleries, leading to the emission of the monomer.

Time-Resolved Fluorescence Measurements. Further insight into the photoluminescence behavior of the solid samples was obtained from time-resolved fluorescence studies. The data summarized in Table 3 show that the decays fit to single (neat viscous oil sample of α2-SO_3H) or double (when incorporated into the LDH) exponential decays (see Experimental Section for further information about $\%C_i$, eq 2).

A decay time of ~430 ps is observed for the pure compound α2-SO_3H (a viscous oil at room temperature). Incorporation of the trisulfonate derivative into the LDH leads to a double exponential decay with two components: a short-lived one associated with the monomer and a long-lived one associated with the aggregate species. A higher excess of the HS surfactant leads to a gradual loss of the aggregate component and the presence of the monomer as the major emissive species (98%), in clear agreement with the observed steady-state data. It is worth noting that the time-resolved data were collected at the shorter emission band (393 nm), and therefore, the C_i values in Table 3 are obtained in the monomer emission region.

4. CONCLUSIONS

A trisulfonated bithiophene (α2-SO_3) has been synthesized and incorporated into a layered double hydroxide host by the direct coprecipitation method. Sole intercalation of α2-SO_3 leads to a well-ordered hybrid assembly with an interlayer spacing of 13.75 Å. However, the material displays a low fluorescence quantum yield due to aggregate-caused quenching (ACQ). A synthetic strategy involving the cointercalation of increasingly higher fractions of the surfactant 1-heptanesulfonate (HS) leads to the gradual emergence of the isolated monomer at the expense of the poorly emissive aggregates, resulting in a remarkable enhancement of the fluorescence emission, in the solid state, from 4% (for the neat compound α2-SO_3H) to 58%. We conclude that the host–guest spatial confinement strategy used here can overcome ACQ with molecular bithiophene fluorophores and obtain solid-state emission, opening a route to highly emissive fluorescent materials.

■ ASSOCIATED CONTENT

Supporting Information

The Supporting Information is available free of charge at https://pubs.acs.org/doi/10.1021/acs.jpcc.1c00240.

Representative SEM images of α2-SO_3-LDH and α2-SO_3(n%)/HS-LDH, with n = 1 and 5%, HSQC NMR and MS spectra of α2-SO_3H, absorption, fluorescence emission and excitation spectra of α_2-SO_3H in water (at different pH values) and methanol, fluorescence decay times and pre-exponential factors of α2-SO_3H in water as a function of pH, excitation spectra of α2-SO_3(n%)/HS-LDH (with n = 100, 5.0, 1.0) with different λ_{em} (PDF)

■ AUTHOR INFORMATION

Corresponding Authors

J. Sérgio Seixas de Melo − *Department of Chemistry, CQC, University of Coimbra, P3004-535 Coimbra, Portugal;* orcid.org/0000-0001-9708-5079; Email: sseixas@ci.uc.pt

Martyn Pillinger − *CICECO - Aveiro Institute of Materials, Department of Chemistry, University of Aveiro, 3810-193 Aveiro, Portugal;* orcid.org/0000-0002-6243-7692; Email: mpillinger@ua.pt

Authors

Estefanía Delgado-Pinar − *Department of Chemistry, CQC, University of Coimbra, P3004-535 Coimbra, Portugal*

Ana L. Costa − *CICECO - Aveiro Institute of Materials, Department of Chemistry, University of Aveiro, 3810-193 Aveiro, Portugal*

Isabel S. Gonçalves − *CICECO - Aveiro Institute of Materials, Department of Chemistry, University of Aveiro, 3810-193 Aveiro, Portugal;* orcid.org/0000-0002-2836-7715

Marta Pineiro − *Department of Chemistry, CQC, University of Coimbra, P3004-535 Coimbra, Portugal;* orcid.org/0000-0002-7460-3758

Complete contact information is available at: https://pubs.acs.org/10.1021/acs.jpcc.1c00240

Notes

The authors declare no competing financial interest.

■ ACKNOWLEDGMENTS

This work was carried out with the support of Centro de Química de Coimbra [FCT (Fundação para a Ciência e a Tecnologia) Ref Nos. UIDB/00313/2020 and UIDP/00313/2020], CICECO - Aveiro Institute of Materials [FCT Ref Nos. UIDB/50011/2020 and UIDP/50011/2020], the COMPETE 2020 Operational Thematic Program for Competitiveness and Internationalization (Project "Hylight", 02/SAICT/2017,

PTDC/QUI-QFI/31625/2017), the CENTRO 2020 Regional Operational Programme (Project "SASCOT", 02/SAICT/2017, PTDC/QUI-QOR/28031/2017), cofinanced by national funds through the FCT/MCTES and the European Union through the European Regional Development Fund (ERDF) under the Portugal 2020 Partnership Agreement. The research leading to these results has received funding from Laserlab-Europe (Grant Agreement No. 284464, EC's Seventh Framework Programme). E.D.-P. thanks the "Concurso de Estímulo ao Emprego Científico" for the Junior Contract CEECIND/04136/2018. The NMR spectrometers of the University of Aveiro are part of the National NMR Network (PTNMR) and are partially supported by Infrastructure Project No. 022161 (cofinanced by the EDRF through COMPETE 2020, POCI and PORL, and the FCT through PIDDAC). NMR data collected at the UC-NMR facility are supported in part by the EDRF through the COMPETE Program and by national funds from the FCT through Grants RECI/QEQ-QFI/0168/2012 and CENTRO-07-CT62-FEDER-002012 and also through support to Rede Nacional de Ressonância Magnética Nuclear (RNRMN) and to Coimbra Chemistry Centre through Grant UID/QUI/00313/2019.

REFERENCES

(1) Kang, S.; Kim, Y. S.; Jeong, J. H.; Kwon, J.; Kim, J. H.; Jung, Y.; Kim, J. C.; Kim, B.; Bae, S. H.; Huang, P. Y.; et al. Enhanced Photoluminescence of Multiple Two-Dimensional van der Waals Heterostructures Fabricated by Layer-by-Layer Oxidation of MoS_2. *ACS Appl. Mater. Interfaces* **2021**, *13*, 1245−1252.

(2) Pina, J.; Burrows, H. D.; Seixas de Melo, J. S. Excited State Dynamics in π-Conjugated Polymers. In *Specialist Periodic Reports in Photochemistry*; Albini, A., Ed.; RSC: Cambridge, 2011; Vol. *39*, pp 30−64.

(3) Pina, J.; Costa, T.; Seixas de Melo, J. S. Dynamics and Photophysics of Oligomers and Polymers. In *Specialist Periodic Reports in Photochemistry*; Albini, A., Ed.; RSC: Cambridge, 2010; Vol. *38*, pp 67−109.

(4) Bianchi, A.; Delgado-Pinar, E.; García-España, E.; Pina, F. 8.23 - Molecular Switching, Logics, and Memories. In *Comprehensive Inorganic Chemistry II*, 2nd ed.; Reedijk, J., Poeppelmeier, K., Eds.; Elsevier: Amsterdam, 2013; pp 969−1037.

(5) Wu, J.; Liu, W.; Ge, J.; Zhang, H.; Wang, P. New Sensing Mechanisms for Design of Fluorescent Chemosensors Emerging in Recent Years. *Chem. Soc. Rev.* **2011**, *40*, 3483−3495.

(6) Chi, Z.; Zhang, X.; Xu, B.; Zhou, X.; Ma, C.; Zhang, Y.; Liu, S.; Xu, J. Recent Advances in Organic Mechanofluorochromic Materials. *Chem. Soc. Rev.* **2012**, *41*, 3878−3896.

(7) Seixas de Melo, J.; Elisei, F.; Gartner, C.; Aloisi, G. G.; Becker, R. S. Comprehensive Investigation of the Photophysical Behavior of Oligopolyfurans. *J. Phys. Chem. A* **2000**, *104*, 6907−6911.

(8) Scherf, U.; Gutacker, A.; Koenen, N. All-Conjugated Block Copolymers. *Acc. Chem. Res.* **2008**, *41*, 1086−1097.

(9) Bäuerle, P. B. J.; Lau, J.; Mark, P. Sulfur-Containing Oligomers. *Electronic Materials: The Oligomer Approach*; Wiley, 1998; pp 105−233.

(10) Celik, D.; Krueger, M.; Veit, C.; Schleiermacher, H. F.; Zimmermann, B.; Allard, S.; Dumsch, I.; Scherf, U.; Rauscher, F.; Niyamakom, P. Performance Enhancement of CdSe Nanorod-Polymer Based Hybrid Solar Cells Utilizing a Novel Combination of Post-Synthetic Nanoparticle Surface Treatments. *Sol. Energy Mater. Sol. Cells* **2012**, *98*, 433−440.

(11) Fichou, D. Structural Order in Conjugated Oligothiophenes and Its Implications on Opto-Electronic Devices. *J. Mater. Chem.* **2000**, *10*, 571−588.

(12) Joe, S. Y.; Ryu, S.; Nguyen, D. C.; Yim, J. H.; Jeong, H.; Ha, N. Y.; Ahn, Y. H.; Park, J. Y.; Lee, S. Contributions of Poly(3-Hexylthiophene) Nanowires to Alteration of Vertical Inhomogeneity of Bulk-Heterojunction Active Layers and Improvements of Light-Harvesting and Power-Conversion Efficiency of Organic Solar Cells. *Org. Electron.* **2017**, *42*, 372−378.

(13) Yin, P. F.; Wang, J. J.; Zhou, Y. Z.; Mao, J.; Qin, W. J.; Qiao, S. Z.; Ling, T.; Du, X. W. Engineering Hollow Electrodes for Hybrid Solar Cells for Efficient Light Harvesting and Carrier Collection. *J. Mater. Chem. A* **2016**, *4*, 17260−17266.

(14) Keller, B.; McLean, A.; Kim, B. G.; Chung, K.; Kim, J.; Goodson, T. Ultrafast Spectroscopic Study of Donor-Acceptor Benzodithiophene Light Harvesting Organic Conjugated Polymers. *J. Phys. Chem. C* **2016**, *120*, 9088−9096.

(15) Honda, S.; Nogami, T.; Ohkita, H.; Benten, H.; Ito, S. Improvement of the Light-Harvesting Efficiency in Polymer/Fullerene Bulk Heterojunction Solar Cells by Interfacial Dye Modification. *ACS Appl. Mater. Interfaces* **2009**, *1*, 804−810.

(16) Johnson, K.; Huang, Y. S.; Huettner, S.; Sommer, M.; Brinkmann, M.; Mulherin, R.; Niedzialek, D.; Beljonne, D.; Clark, J.; Huck, W. T. S.; Friend, R. H. Control of Intrachain Charge Transfer in Model Systems for Block Copolymer Photovoltaic Materials. *J. Am. Chem. Soc.* **2013**, *135*, 5074−5083.

(17) Pina, J.; Rodrigues, A. C. B.; Alnady, M.; Dong, W. Y.; Scherf, U.; de Melo, J. S. S. Restricted Aggregate Formation on Tetraphenylethene-Substituted Polythiophenes. *J. Phys. Chem. C* **2020**, *124*, 13956−13965.

(18) Costa, A. L.; Gomes, A. C.; Pillinger, M.; Gonçalves, I. S.; Pina, J.; Seixas de Melo, J. S. Insights into the Photophysics and Supramolecular Organization of Congo Red in Solution and the Solid State. *ChemPhysChem* **2017**, *18*, 564−575.

(19) Karsenti, E. Self-Organization in Cell Biology: A Brief History. *Nat. Rev. Mol. Cell Biol.* **2008**, *9*, 255−262.

(20) Philp, D.; Stoddart, J. F. Self-Assembly in Natural and Unnatural Systems. *Angew. Chem., Int. Ed. Engl.* **1996**, *35*, 1154−1196.

(21) Kasha, M.; Rawls, H. R.; El-Bayoumi, M. A. Exciton Model in Molecular Spectroscopy. *Pure Appl. Chem.* **1965**, *11*, 371−392.

(22) Aida, T.; Meijer, E. W.; Stupp, S. I. Functional Supramolecular Polymers. *Science* **2012**, *335*, 813−817.

(23) Martín, C.; Piatkowski, P.; Cohen, B.; Gil, M.; Navarro, M. T.; Corma, A.; Douhal, A. Ultrafast Dynamics of Nile Red Interacting with Metal Doped Mesoporous Materials. *J. Phys. Chem. C* **2015**, *119*, 13283−13296.

(24) Yamaguchi, A.; Amino, Y.; Shima, K.; Suzuki, S.; Yamashita, T.; Teramae, N. Local Environments of Coumarin Dyes within Mesostructured Silica−Surfactant Nanocomposites. *J. Phys. Chem. B* **2006**, *110*, 3910−3916.

(25) Costa, A. L.; Gomes, A. C.; Pereira, R. C.; Pillinger, M.; Gonçalves, I. S.; Pineiro, M.; Seixas de Melo, J. S. Interactions and Supramolecular Organization of Sulfonated Indigo and Thioindigo Dyes in Layered Hydroxide Hosts. *Langmuir* **2018**, *34*, 453−464.

(26) Gago, S.; Costa, T.; de Melo, J. S.; Gonçalves, I. S.; Pillinger, M. Preparation and Photophysical Characterisation of Zn-Allayered Double Hydroxides Intercalated by Anionic Pyrene Derivatives. *J. Mater. Chem.* **2008**, *18*, 894−904.

(27) Nguyen, T. K. N.; Dumait, N.; Grasset, F.; Cordier, S.; Berthebaud, D.; Matsui, Y.; Ohashi, N.; Uchikoshi, T. Zn−Al Layered Double Hydroxide Film Functionalized by a Luminescent Octahedral Molybdenum Cluster: Ultraviolet−Visible Photoconductivity Response. *ACS Appl. Mater. Interfaces* **2020**, *12*, 40495−40509.

(28) Mishra, G.; Dash, B.; Pandey, S. Layered Double Hydroxides: A Brief Review from Fundamentals to Application as Evolving Biomaterials. *Appl. Clay Sci.* **2018**, *153*, 172−186.

(29) Evans, D. G.; Slade, R. C. T. Structural Aspects of Layered Double Hydroxides. In *Layered Double Hydroxides*; Duan, X., Evans, D. G., Eds.; Springer: Berlin, Heidelberg, 2006; pp 1−87.

(30) Zhao, Q.; Chang, Z.; Lei, X.; Sun, X. Adsorption Behavior of Thiophene from Aqueous Solution on Carbonate- and Dodecylsul-

https://doi.org/10.1021/acs.jpcc.1c00240
J. Phys. Chem. C 2021, 125, 8294−8303

fate-Intercalated ZnAl Layered Double Hydroxides. *Ind. Eng. Chem. Res.* **2011**, *50*, 10253−10258.
(31) Tronto, J.; Sanchez, K. C.; Crepaldi, E. L.; Naal, Z.; Klein, S. I.; Valim, J. B. Synthesis, Characterization and Electrochemical Study of Layered Double Hydroxides Intercalated with 2-Thiophenecarboxylate Anions. *J. Phys. Chem. Solids* **2004**, *65*, 493−498.
(32) Tronto, J.; Pinto, F. G.; da Costa, L. M.; Leroux, F.; Dubois, M.; Valim, J. B. In Situ Oligomerization of 2-(Thiophen-3-yl)Acetate Intercalated into Zn_2Al Layered Double Hydroxide. *J. Solid State Chem.* **2015**, *221*, 391−397.
(33) Costa, A. L.; Gomes, A. C.; Pillinger, M.; Gonçalves, I. S.; Seixas de Melo, J. S. Controlling the Fluorescence Behavior of 1-Pyrenesulfonate by Cointercalation with a Surfactant in a Layered Double Hydroxide. *Langmuir* **2015**, *31*, 4769−4778.
(34) Magde, D.; Wong, R.; Seybold, P. G. Fluorescence Quantum Yields and Their Relation to Lifetimes of Rhodamine 6G and Fluorescein in Nine Solvents: Improved Absolute Standards for Quantum Yields. *Photochem. Photobiol.* **2002**, *75*, 327−334.
(35) Seixas de Melo, J.; Fernandes, P. F. Spectroscopy and Photophysics of 4- and 7-Hydroxycoumarins and Their Thione Analogs. *J. Mol. Struct.* **2001**, *565*−*566*, 69−78.
(36) Pina, J.; Seixas de Melo, J. S.; Burrows, H. D.; Maçanita, A. L.; Galbrecht, F.; Bunnagel, T.; Scherf, U. Alternating Binaphthyl-Thiophene Copolymers: Synthesis, Spectroscopy, and Photophysics and Their Relevance to the Question of Energy Migration Versus Conformational Relaxation. *Macromolecules* **2009**, *42*, 1710−1719.
(37) Striker, G.; Subramaniam, V.; Seidel, C. A. M.; Volkmer, A. Photochromicity and Fluorescence Lifetimes of Green Fluorescent Protein. *J. Phys. Chem. B* **1999**, *103*, 8612−8617.
(38) Rodrigues, A. C. B.; Geisler, I. S.; Klein, P.; Pina, J.; Neuhaus, F. J. H.; Dreher, E.; Lehmann, C. W.; Scherf, U.; Seixas de Melo, J. S. Designing Highly Fluorescent, Arylated Poly(Phenylene Vinylene)s of Intrinsic Microporosity. *J. Mater. Chem. C* **2020**, *8*, 2248−2257.
(39) CrystalMaker Software. CrystalMaker(R): A Crystal and Molecular Structures Modelling Program for Mac and Windows, 9: Oxford, UK.
(40) Delgado-Pinar, E.; Pineiro, M.; Sérgio Seixas de Melo, J. A Water-Soluble Bithiophene with Increased Photoluminescence Efficiency and Metal Recognition Ability. *Dalton Transactions* **2020**, *49*, 12319−12326.
(41) Groom, C. R.; Bruno, I. J.; Lightfoot, M. P.; Ward, S. C. The Cambridge Structural Database. *Acta Crystallogr., Sect. B: Struct. Sci., Cryst. Eng. Mater.* **2016**, *72*, 171−179.
(42) Einkauf, J. D.; Ortega, R. E.; Mathivathanan, L.; de Lill, D. T. Nitroaromatic Sensing with a New Lanthanide Coordination Polymer $[Er_2(C_{10}H_4O_4S_2)_3(H_2O)_6]_n$ Assembled by 2,2′-Bithiophene-5,5′-Dicarboxylate. *New J. Chem.* **2017**, *41*, 10929−10934.
(43) Becker, R. S.; Seixas de Melo, J.; Maçanita, A. L.; Elisei, F. Comprehensive Evaluation of the Absorption, Photophysical, Energy Transfer, Structural, and Theoretical Properties of α-Oligothiophenes with One to Seven Rings. *J. Phys. Chem.* **1996**, *100*, 18683−18695.
(44) Lanzani, G. Molecular Exciton. In *The Photophysics Behind Photovoltaics and Photonics*; Lanzani, G., Ed.; Wiley-VCH Verlag GmbH & Co. KGaA: Weinheim, Germany, 2012; pp 35−52.

https://doi.org/10.1021/acs.jpcc.1c00240
J. Phys. Chem. C 2021, 125, 8294−8303